REVIEW

Perovskite in Earth's deep interior

Kei Hirose,[1,2]* Ryosuke Sinmyo,[1,2] John Hernlund[1]

Silicate perovskite-type phases are the most abundant constituent inside our planet and are the predominant minerals in Earth's lower mantle more than 660 kilometers below the surface. Magnesium-rich perovskite is a major lower mantle phase and undergoes a phase transition to post-perovskite near the bottom of the mantle. Calcium-rich perovskite is proportionally minor but may host numerous trace elements that record chemical differentiation events. The properties of mantle perovskites are the key to understanding the dynamic evolution of Earth, as they strongly influence the transport properties of lower mantle rocks. Perovskites are expected to be an important constituent of rocky planets larger than Mars and thus play a major role in modulating the evolution of terrestrial planets throughout the universe.

Perovskite-type crystals, or perovskites, are famous for their chemical flexibility and wide range of industrial applications as ferroelectrics, piezoelectrics, superconductors, and photovoltaic materials. The mineral perovskite, named for Russian mineralogist Lev Perovski in 1839, has a chemical formula $CaTiO_3$ and was discovered in the southern Ural Mountains. Perovskite, for researchers studying Earth, refers to the isostructural $MgSiO_3$ or $CaSiO_3$ minerals (called Mg-perovskite or Ca-perovskite hereafter) believed to make up the bulk of the lower mantle. Intact Mg-perovskite crystals have also been discovered in shocked veins in the Tenham meteorite (*1*, *2*) and named "bridgmanite" after pioneering high-pressure physicist Percy Bridgman.

In ABX_3-type materials with ideal perovskite structure, ions A and X comprise close-packed face-centered cubic structures, with A ions sited in the larger spaces between corner-linked BX_6 octahedra (Fig. 1, left). These well-packed structures are favored at high pressure, and major elements in terrestrial planets (Mg, Si, and O) form Mg-perovskite under the conditions prevailing in their deep interiors. Mg-perovskite is stable above ~23 GPa and was first synthesized in the 1970s in the laboratory (*3*, *4*). Mg-perovskite is a predominant phase in Earth's lower mantle (depth of 660 to 2600 to 2890 km) and is also expected to be an abundant mineral in other terrestrial planets larger than Mars. The formation of Mg-perovskite develops an important dynamical boundary inside planets because it greatly increases density and viscosity (*5*).

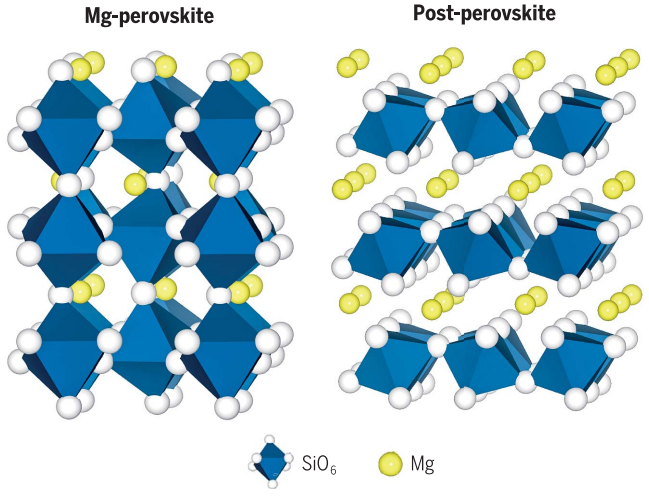

Fig. 1. Crystal structures of $MgSiO_3$ perovskite and post-perovskite. SiO_6 coordination polyhedra of oxygen atoms (white spheres) around silicon atoms are shown as blue octahedra, and the Mg ions are shown as yellow spheres. Both are orthorhombic crystal lattices with space group *Pbnm* for Mg-perovskite and *Cmcm* for post-perovskite.

Mineralogy of Earth's lower mantle and post-perovskite phase transition

Seismology shows a layered structure in Earth's mantle, with marked velocity differences between the upper mantle (to 410-km depth), transition zone (410- to 660-km depth), lower mantle (660- to 2600-km depth), and lowermost mantle (2600- to 2890-km depth). Pyrolite is a theoretical chemical composition and similar to those of least-differentiated upper mantle rocks. Pyrolite is often assumed to represent a typical composition for the entire mantle because phase transitions in primary minerals that occur in a pyrolitic composition align with the layered structure of the mantle (Fig. 2A). However, seismic-wave speeds are not well explained by a pyrolitic mantle, possibly suggesting that Earth's mantle is an inhomogeneous mixture of basaltic and harzburgitic rocks (*6*).

The occurrence of Mg-perovskite at about 660-km depth is readily imaged by seismic waves as a global discontinuity. In a pyrolitic mantle, Mg-perovskite is formed from both the primary and secondary minerals in the transition zone, $(Mg,Fe)_2SiO_4$ ringwoodite (a spinel-type mineral) and (Fe,Al)-bearing $MgSiO_3$ majorite (from the garnet family), upon increasing pressure (Fig. 2B). As a consequence, Mg-perovskite constitutes a large proportion of the lower mantle, coexisting with (Mg,Fe)O ferropericlase and Ca-perovskite (~80, ~15, and ~5 volume % in pyrolite, respectively). The formation of Mg-perovskite is associated with an increase in the coordination number of Si from four to six. This leads to a negative Clapeyron (dP/dT) slope, where P is pressure and T is temperature, because the increase in the coordination number increases first-neighbor Si–O distance and thus increases entropy (*7*). The Clapeyron slope of the post-spinel phase boundary (ringwoodite to Mg-perovskite with ferropericlase) was first determined to be –3 MPa K^{-1} with a conventional "quench" method in a multianvil press (Fig. 2B), consistent with the seismologically determined dP/dT slope of the 660-km boundary (*8*). This value has been controversial (–0.4 to –3 MPa K^{-1}), because precise determination of pressure at high temperature is usually dependent on the *P-V-T* equation of state of an internal standard, but the accuracy and consistency of the equation of state for various kinds of standards are matters of debate (*9*).

The incorporation of a relatively small Mg^{2+} ion between the SiO_6 octahedra in Mg-perovskite causes an orthorhombic distortion of the typical cubic perovskite structure (Fig. 1, left). This distortion is enhanced with increasing pressure (fig. S1) and eventually leads to a phase transition into "post-perovskite" (Fig. 1, right) above 120 GPa (Fig. 2C) (*10*–*12*). The lowermost mantle (D″ layer) is marked by a shear velocity jump intermittently around 2600-km depth that matches 120 GPa, mainly at relatively cold regions. The calculated sound velocity of post-perovskite is consistent with the seismological observations of an ~3% increase in shear velocity and almost no change in compressional velocity for discontinuities imaged in the D″ layer (*13*). Nevertheless, the effects of minor components such as FeO, Fe_2O_3, and Al_2O_3 on the pressure and the width of the transition are controversial (Fig. 2C). Ohta *et al.* (*14*) and Fiquet *et al.* (*15*) reported a sharp (≤5-GPa width) boundary in pyrolite at 120 to 138 GPa and 2500 to 3500 K, consistent with the seismic velocity jump observed around 2600-km depth. Conversely, the phase transition was found to occur over a very wide (>20 GPa) pressure range with the incorporation of Fe and Al (*16*). Grocholski *et al.* (*17*) found that the post-perovskite phase transition does not occur in pyrolite at mantle pressures, but may occur in basalt and harzburgitic mantle bulk compositions.

[1]Earth-Life Science Institute, Tokyo Institute of Technology, Meguro, Tokyo 152-8550, Japan. [2]Department of Earth and Planetary Science, Graduate School of Science, The University of Tokyo, Bunkyo, Tokyo 113-0033, Japan.
*Corresponding author. Email: kei@elsi.jp

Dynamics in the lower mantle

The negative Clapeyron slope of the post-spinel transition resists penetration of mantle convection between the transition zone and the lower mantle. This, combined with a viscosity increase, causes the stagnation of subducting pieces of former oceanic lithosphere called "slabs" around 660 km depth (*8*). Slab stagnation occurs also at ~1000 km depth, corresponding to a viscosity "hill" (*18*) possibly related to iron spin crossover (*19*) or iron depletion in Mg-perovskite (*20*). Slabs may also stagnate on the top of bridgmanite (Mg-perovskite)–enriched ancient mantle structures (BEAMS) (*21*) (Fig. 3). By contrast, upwelling hot plumes do not seem to stagnate at the 660-km boundary, possibly because Mg-perovskite transforms into majorite at high temperatures (>2100 K) with a positive Clapeyron slope (*22*) (Fig. 2B). Conversely, the post-perovskite phase transformation in the lowermost mantle exhibits a large positive dP/dT slope and thus assists mantle convection (*11*, *12*, *23*). If post-perovskite is present in plume-upwelling regions, the phase transition to Mg-perovskite plays an important role because it occurs near the lowermost mantle thermal boundary layer. The phase transition therefore destabilizes the lowermost mantle and enhances the number of plumes, possibly also increasing the temperature of the whole mantle by a few hundred degrees (*24*).

Laboratory experiments have demonstrated that Mg-perovskite is much more rigid than upper mantle and transition-zone minerals and is three orders of magnitude more viscous than coexisting MgO periclase (*5*). Indeed, the viscosity of the lower mantle based on geodetic measurements has been estimated to be at least one order of magnitude higher than shallower levels and is often assumed to be more viscous by a factor of ~30 (*25*). If periclase can be interconnected between stronger Mg-perovskite grains to weaken the whole rock, this would lead to complex and interesting behaviors. In a well-connected state, changes in the iron spin state in (Mg,Fe)O ferropericlase could influence the viscosity of the weak phase and manifest themselves as a higher-viscosity layer in the lower mantle (*19*). The transformation into a post-spinel assemblage (Mg-perovskite with periclase) reveals little interconnectivity between periclase grains (*26*). However, recent deformation the post-spinel assemblage suggest that periclase grains might become interconnected and weaken the assemblage at larger strains, and could lead to dramatic weakening. This kind of strain-weakening behavior is important because it may give rise to shear localization in the lower mantle, in which narrow zones of intense deformation separate large quiescent regions that undergo relatively little deformation (see below). Strain causes weakening that in turn begets more strain, leading to a runaway effect similar to what is thought to accommodate plate tectonics. In the deepest portions of Earth's mantle, post-perovskite is expected to be much weaker than perovskite owing to its layered crystal structure (*28*). Because it is stabilized at lower temperatures, such weak post-perovskite may weaken rocks that would otherwise be highly viscous owing to the usual influence of cooler temperatures on viscosity.

Chemical and physical properties of mantle perovskite

Impurities, such as Al and Fe, can strongly influence the behavior of Mg-perovskite in Earth's lower mantle. Although iron is predominantly Fe^{2+} in the upper mantle and the transition zone, it is able to coexist as Fe^{0}, Fe^{2+}, and Fe^{3+} in the lower mantle. This is in part because Al^{3+} is preferentially accommodated into the small Si^{4+} site (B site) in Mg-perovskite, which induces the disproportionation of Fe^{2+} ($\rightarrow Fe^{3+} + Fe^{0}$) as Fe^{3+} enters the Mg^{2+} site (A site) in order to maintain a charge balance. Indeed, relics of natural Mg-perovskite found in diamonds contain a large amount of Fe^{3+} (*29*), although the diamonds are formed under environments that may not represent the typical redox conditions of the mantle (*30*). Recent experiments found that iron in Mg-perovskite is dominantly Fe^{2+} at 40 to 70 GPa, whereas $Fe^{3+}/(Fe^{2+} + Fe^{3+})$ = ~0.6 in other pressure ranges (*20*). Because ferrous iron is preferentially accommodated into coexisting ferropericlase, it may cause iron depletion in Mg-perovskite at 1100- to 1700-km depth. Shim and others speculate that the observed mid–lower mantle viscosity anomaly (*20*) might be a result of iron depletion in Mg-perovskite.

The spin state of iron in Mg-perovskite changes from high to low spin with increasing pressure. Such an iron spin crossover was first discovered in (Mg,Fe)O ferropericlase at the pressure range of the lower mantle (*31*) and has important geophysical implications (*32*). The iron spin state in Mg-perovskite is more complicated owing to multiple valence states and crystallographic sites. Fe^{2+} is accommodated only in the A site and undergoes the spin crossover above ~30 GPa from high spin to what was identified as intermediate spin (*33*, *34*). However, a component that was assigned to intermediate-spin Fe^{2+} in Mössbauer spectra may be explained by high-spin Fe^{2+} in the distorted A site (*35*). Conversely, Fe^{3+} that occupies the B site undergoes high-spin to low-spin crossover above 30 GPa (*36*). The valence and spin states control the partitioning of iron between Mg-perovskite and ferropericlase (*31*). Recent work suggests that it changes around 60 GPa because of the spin crossover (*37*), but the effect is much smaller than previously thought. Recent approaches, such

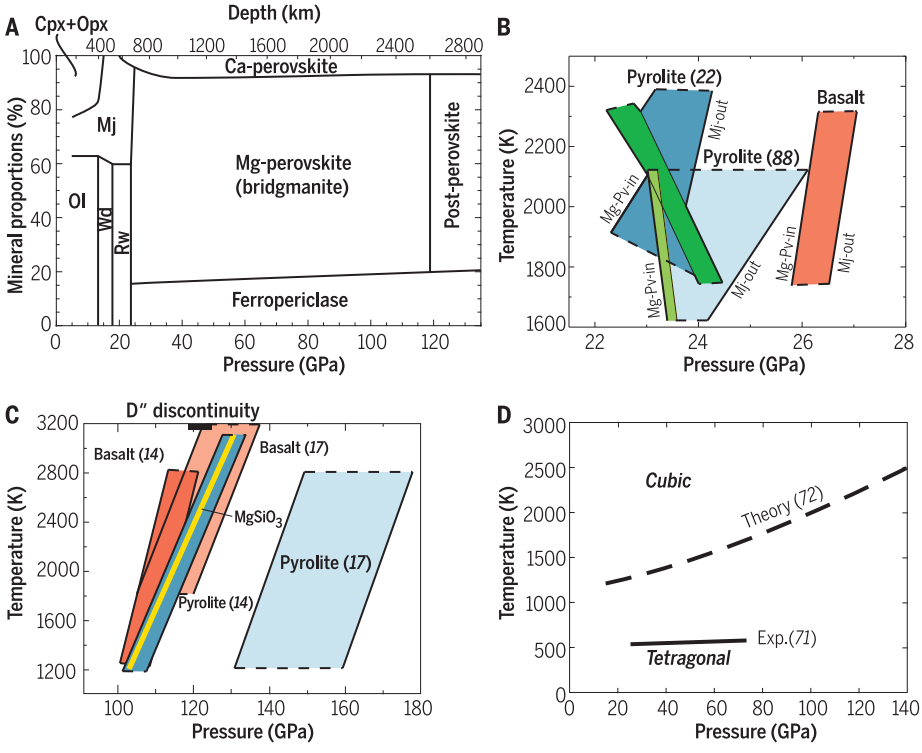

Fig. 2. Phase proportions and phase transition boundaries in Earth's lower mantle. (**A**) Mineral proportions in pyrolytic mantle rocks. Ol, olivine; Wd, wadsleyite; Rw, ringwoodite; Cpx, clinopyroxene; Opx, orthopyroxene; Mj, majorite (garnet). (**B**) Phase transition boundaries near 660-km depth in pyrolitic mantle and basalt compositions (*22*, *88*). Mg-perovskite is formed in pyrolite by both post-spinel (ringwoodite to Mg-perovskite and ferropericlase) (green) and majorite-perovskite transition (blue). Majorite transforms into Mg-perovskite in basalt (orange). Two-phase coexisting regions are shown as bands. Pv, perovskite. (**C**) Phase boundary between Mg-perovskite and post-perovskite is illustrated for $MgSiO_3$ (yellow line) (*23*), pyrolytic mantle (blue), and subducted basalt (orange) (*14*, *17*). (**D**) Phase transition boundary in Ca-perovskite. Both theory (*72*) and experiment (*71*) demonstrated tetragonal to cubic phase transition at high temperatures.

as theoretical predictions (*38*) and the observation of natural samples (*39*), provide further insight about changes in iron partitioning.

Mg-perovskite is much less compressible (bulk modulus at ambient condition, K_0 = 258 GPa) (*40*) than coexisting ferropericlase (K_0 = 158 GPa) (*41*). The measured Vickers hardness of Mg-perovskite is 18 GPa, several factors higher than that of olivine, enstatite, and periclase (*42*). The effects of impurities (Fe^{2+}, Fe^{3+}, and Al^{3+}) on K are not yet clear (*43*, *44*), likely because of the multiple site distributions and electronic states of iron. Unlike the remarkable volumetric and bulk modulus decrease of ferropericlase from the spin crossover, even at high temperatures, the Fe^{3+} spin transition in Mg-perovskite has little effect upon its compression behavior (*43*, *44*). The combination may explain mid–lower mantle seismic anomalies without introducing compositional heterogeneity (*32*).

The thermal properties of Mg-perovskite are key to understanding the thermal structure of the lower mantle and the heat transported away from the core by mantle convection. The thermal expansion coefficient and heat capacity of Mg-perovskite largely determine the adiabatic temperature profile in the lower mantle (*45*). Although the heat capacity is difficult to measure at high *P-T*, theory predicts an almost constant value at >1000 K regardless of pressure (*46*). Recent progress also includes the measurement of thermal diffusivity of Mg-perovskite (*47*, *48*), from which the thermal conductivity of the lowermost mantle was determined to be about 10 W m^{-1} K^{-1}. Lattice thermal conductivity is diminished at higher temperature but enhanced at higher pressure (*47*, *48*), and thus, the thermal conductivity may remain similar throughout the lower mantle. The contribution of radiative thermal transport through Mg-perovskite still remains controversial (*49*, *50*). Combining such thermal conductivity with temperature gradients at the base of the mantle, which may be steeper than the post-perovskite phase transition boundary (*51*), a global heat flow across the core–mantle boundary (CMB) is estimated to be more than 7 TW (*23*), suggesting rapid cooling of Earth's core. Depending on the pressure scale (*52*), the Clapeyron slope of the boundary can be smaller, leading to the larger CMB heat flow.

The sound velocity of Mg-perovskite has been determined at lower mantle pressures by Brillouin scattering measurements (*53*, *54*) and theoretical calculations (*55*, *56*). A comparison of shear and compressional velocities of Mg-perovskite and ferropericlase with seismological observations can test the pyrolitic mantle compositional model. Murakami *et al.* (*53*) argued that Mg-perovskite constitutes more than 90% in lower mantle rocks, although this may be an overestimate (*57*). It indicates a chondritic-like Mg/Si ratio close to 1.0, which is different from the observed value of 1.3 in the pyrolitic upper mantle. Considering the large volume of the lower mantle, a smaller Mg/Si ratio would help reconcile the bulk silicate mantle with the chondritic compositional models for Earth's formation (Box 1).

Electrical conductivity is an observable property of Earth's interior obtained from temporal fluctuations in the magnetic field (*58*). Conductivity is sensitive to water and iron content, so it provides specific information on the chemistry of the mantle. The conductivity of (Fe,Al)-bearing natural Mg-perovskite measured in a multianvil press is higher than those of transition-zone minerals because of a greater sensitivity to temperature (*59*). Although the influence of the spin crossover in Fe^{3+} is controversial (*60*, *61*), it should diminish electrical conductivity as is found in ferropericlase, owing to the reduction in the number of unpaired electrons. The discrepancy surrounding the impact of the spin crossover either allows for the simple pyrolytic composition (*61*) or requires the inclusion of subducted basaltic crust in the lower mantle (*60*). Post-perovskite with a layered crystal structure (Fig. 1B) exhibits more than two orders of magnitude higher conductivity than Mg-perovskite (*62*). This should enhance electromagnetic coupling between the lowermost mantle and the liquid outer core, which may help to explain variations in day length on decadal time scales (*63*).

The presence of H_2O in crystal lattice affects melting temperature, viscosity, and electrical conductivity to larger extents. Multianvil experiments (*64*) reported 8000 parts per million (ppm)

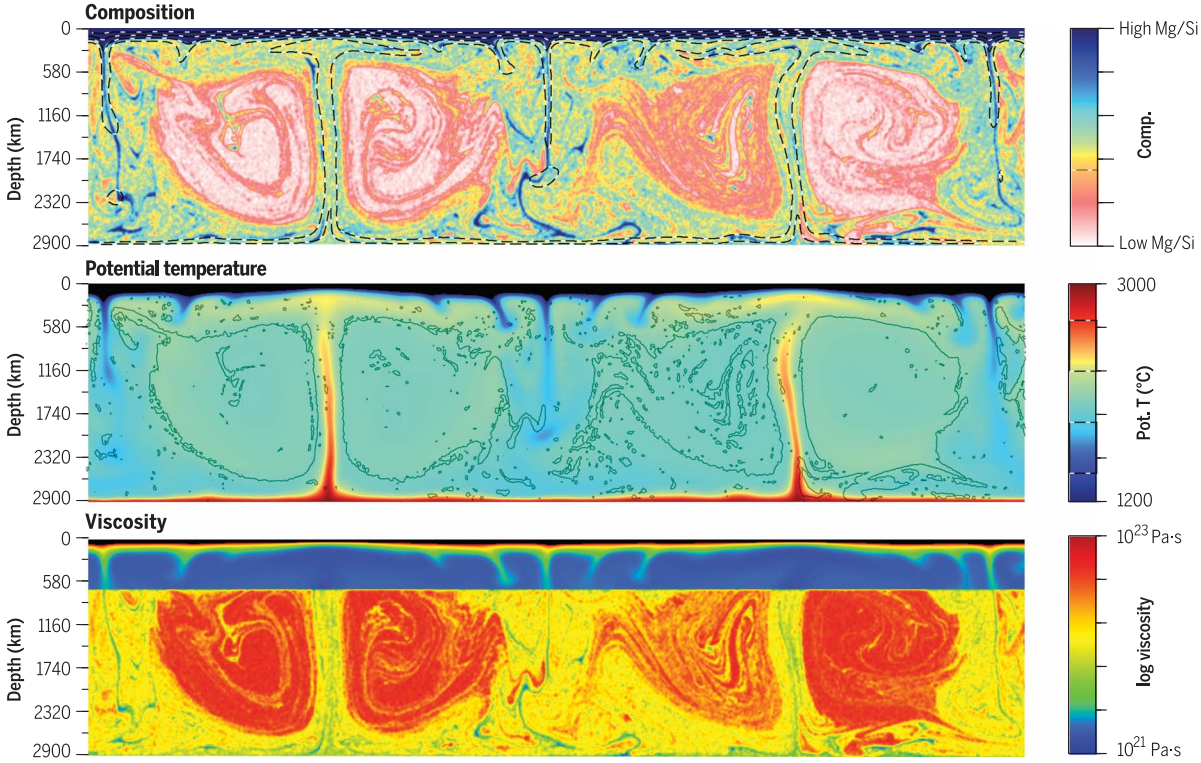

Fig. 3. Mg-perovskite–enriched ancient mantle structures in the lower mantle. Numerical simulations (*21*) demonstrated that Mg-perovskite–enriched (low Mg/Si) domains are strong and organize mantle convection patterns. They are encapsulated by weaker pyrolitic (high Mg/Si) material, which circulates between the shallow and deepest mantle through channels between the strong domains. The Mg-perovskite–rich domains are unmixed throughout the history of Earth, which may reconcile the fixed positioning of plume centers and the slab stagnation at ~1000-km depth and provide a reservoir to host primordial geochemical signatures.

H_2O in Al-bearing Mg-perovskite, suggesting that the lower mantle is potentially a large water reservoir (*65*). These experiments are consistent with geochemical estimates of high volatile concentrations with up to ~1000 ppm H_2O in the source mantle for oceanic island basalts, possibly originating from the lower mantle (*66*). Conversely, earlier experiments (*67*) and calculations found a much lower solubility of water in Mg-perovskite (a concentration of 100 ppm or less) and suggested that the high concentrations of H_2O measured in other experiments were present in fluid inclusions instead of dissolved into the mineral itself. Al-bearing post-perovskite was predicted to accommodate 5 to 10 times more H_2O than Mg-perovskite (*68*). Townsend and others (*68*) argued that the dehydration of post-perovskite upon transformation to Mg-perovskite at high-temperature regions induces partial melting, which is observed as an ultralow-velocity zone (*69*). Experiments also suggested high solubilities of noble gases in Mg-perovskite: up to ~1 weight % (wt %) He and Ar and some Kr, but not Xe (*70*).

$CaSiO_3$ perovskite: A host of trace elements

Because the ionic radius of Ca^{2+} is much larger than that of Mg^{2+}, Mg-perovskite forms a very limited solid solution with $CaSiO_3$ component, and therefore, Ca-perovskite is present as a separate phase. The ratio between the ionic radii of A and B in ABX_3-type perovskites, called "tolerance factor," determines the type of perovskite structures proposed by Victor Goldschmidt. The structure of Ca-perovskite exhibits cubic symmetry at the high temperatures of the lower mantle (>1900 K) (*45*) but is possibly distorted in subducted cold materials (*71*, *72*) (Fig. 2D). Theory predicted that Ca-perovskite transforms into post-perovskite–type phase or dissociates into CaO and SiO_2, depending on temperature, above 500 GPa (*73*).

Ca-perovskite is proportionally minor but is likely the predominant host for large ion lithophile (silicate-loving) elements (LILE) in the lower mantle (*74*, *75*). Because of the high Ca-perovskite/melt partition coefficients (>10 for many of the LILE), partial melting in the lower mantle causes strong enrichment of LILE in Ca-perovskite–bearing solid residues. Although the stability of Ca-perovskite above the solidus temperature is very small in a pyrolite composition, it is one of the major constituents (~20 volume %) and the last melting phase in basaltic crusts subducted into the lower mantle. Indeed, the melting temperature of basaltic materials is lower than that of pyrolite (*76*), and if they undergo partial melting at the CMB, Ca-perovskite–rich residues are formed with LILE-enriched characters. Once they are upwardly entrained in plumes, melting of such blocks in the shallow mantle could produce characteristic geochemical signatures in magmas; strong enrichment in Th and U relative to Pb in Ca-perovskite will result in radiogenic Pb isotopes. Incorporation of U and Th into Ca-perovskite has also been examined by using theoretical calculations (*77*).

Perspective: Challenges and new views

The CMB temperature is about 4000 K, but many chemical and physical properties of Mg-perovskite are known only for moderate temperatures. For example, thermal conductivity was determined to 1073 K (*47*), and sound velocity (*53*), electrical conductivity (*60*), and iron partitioning (*37*) were obtained only below ~2700 K. In addition, most measurements at lower mantle *P-T* conditions were performed in a laser-heated diamond-anvil cell (DAC), with an intrinsically large temperature gradient and different sample geometries, which might be major sources of inconsistency for results reported by different groups. Advanced experiments with different heating techniques—such as multianvil apparatus with sintered-diamond cubes (*26*), resistance-heated DAC, or shockwaves—will help improve understanding of the nature of the bottom of the mantle that controls the dynamics and evolution of both mantle and core. Rheological properties of Mg-perovskite will also be examined at deep lower mantle *P-T* conditions in the near future, with advanced experimental techniques using, for example, the rotational Drickamer apparatus (*27*), the Kawai-type deformation-DIA apparatus (*78*), and rotation DAC (*79*).

$MgSiO_3$-rich perovskite (bridgmanite) is...

1. **Most abundant mineral inside Earth**
   Nearly 50% of bulk Earth in volume
2. **Only stable at high pressure**
   >23 GPa (=230,000 atmospheric pressure)
3. **Less compressive**
   Bulk modulus at 1 bar = 258 GPa
   (higher than Al_2O_3 corundum)
4. **Hard**
   Vickers hardness = 18 GPa
   (as high as corundum)

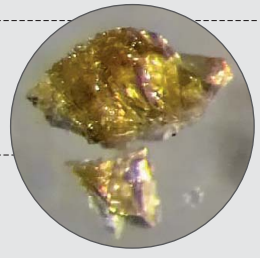

5. **Moderately transparent**
   Absorption coefficient ~10 to 50 mm^{-1} at λ = 600 nm, ~40 GPa, 300 K
6. **Moderately conductive**
   Electrical conductivity ~ 1 S/m at 25 GPa, 1873 K
   Thermal conductivity ~ 10 W m^{-1} K^{-1} at 25 GPa, 300 K
7. **A potential reservoir of volatiles**
   Up to ~ 0.8 wt % H_2O and ~ 1 wt % noble gases

Characteristics of $MgSiO_3$ perovskite.

Geodynamical models suggest that the whole mantle becomes well-mixed by mantle convection over ~100 million–year time scales with the assumption of a simple viscous rheology (*21*). The mantle is in a fluid dynamical regime characterized by relatively high convective vigor and a close balance between viscous and buoyancy forces, and for which viscous entrainment and mixing is highly effective. However, geochemical evidence directly contradicts this, as it points to the existence of isotopically distinct domains in Earth's interior that should have been isolated since Earth's formation (*80*–*82*). Many clues suggest that these isolated reservoirs reside in Earth's lower mantle, and therefore the dynamics of the lower mantle, and by extension the transport properties of Mg-perovskite, must be reexamined in greater detail.

A simple model to delay mixing of geochemically distinct domains is through variations in the Mg/Si ratio of rocks circulating through the deep mantle, which give rise to viscosity variations that organize the large-scale pattern of convection. The viscosity variations relate to the relative proportions of Mg-perovskite to ferropericlase as the Mg/Si ratio changes. The resulting dynamical regime results in isolated strong BEAMS separated by channels of higher-Mg/Si (relatively weak) rocks that readily deform and circulate between the shallow and deep mantle (Fig. 3) (*21*). Such BEAMS may help to solve the "missing silicon paradox" (Box 1), in addition to hosting other isotopically distinct material since the time of early Earth. The potential for strain weakening through the interconnection of the weaker periclase (*27*) may amplify this picture by shear-localizing rheology that would help isolate compositionally distinct domains.

Perovskite should also be an important constituent in other terrestrial planets if their rocky mantles contain substantial volumes above ~23 GPa. Venus, being similar in size and mass to Earth, should also host Mg-perovskite as its most abundant mineral phase. The base of Mars' mantle, on the other hand, is estimated to be 19 to 27 GPa (*83*), and it is unknown whether any Mg-perovskite is stable inside the red planet (*84*). Larger terrestrial-like planets that exist around other stars may find large portions of their mantles above ~100 GPa, well beyond the stability field of Mg-perovskite. Nevertheless, the Mg-perovskite–bearing portion of every terrestrial planet could play a limiting role in the dynamical evolution of the planet, particularly if it is highly enriched in Mg-perovskite, because the high viscosity of this phase moderates the mantle convection conveyor belt that circulates material between the surface and deep interior.

If a planet hosts too much Mg-perovskite, and its rheology is thereby too strong to permit efficient cooling by mantle convection, heat will build up in the interior, owing to ambient radioactivity, and raise the temperature, thus softening the rock until it can permit convective flows and release the excess heat (*85*). Thus, terrestrial

PHOTO CREDIT: TAKAYUKI ISHII

Box 1. The chemical composition of Earth.

The bulk Earth is considered to be similar in composition to chondrites (primitive meteorites), with the exception of volatile elements (*89*), because the chondrites coming from the asteroid belt have compositions that are almost the same as the solar composition. However, the typical composition of Earth's uppermost mantle (pyrolite) is different from that of the silicate part of the chondrites; Mg/Si molar ratio is ~1.3 for the former and 1.0 for the latter. Indeed, a primary mineral is Mg_2SiO_4-rich olivine in the upper mantle, whereas a primary mineral is $MgSiO_3$-rich enstatite in chondrites. This is the missing silicon paradox. In order to reconcile the bulk Earth Mg/Si ratio with the chondritic and solar values, it has been argued that 6 to 12 wt % Si is present in the core (*89*, *90*), as supported by the $^{30}Si/^{28}Si$ isotopic composition ($\delta^{30}Si$) of Earth's mantle, which is higher than those of chondrites (*90*). The recent work by Dauphas *et al*. (*91*) estimated a more modest amount of Si (3.6 wt %) in Earth's core, considering the bulk planetary-scale variations in Mg/Si and $\delta^{30}Si$. They argued that such variations were caused by the fractionation of forsterite (Mg/Si = 2) in the solar nebula, which can vary the Mg/Si ratio, and thus mantle viscosity, in planetary bodies. Alternatively, it is also possible that Earth's lower mantle has a chondritic Mg/Si ratio different from that observed in the upper mantle. This means that the lower mantle is composed almost entirely of Mg-perovskite (*21*, *53*), which could happen if a magma ocean extended to the deep mantle and crystallized it as a liquidous phase (*92*).

mantles containing a higher proportion of Mg-perovskite are expected to be hotter than those bearing enough periclase to allow for substantial weakening of the rock. If the elevated temperatures are high enough to cause partial melting of an assemblage of Mg-perovskite with a minor amount of periclase, the eutectic melt will have a relatively higher Mg/Si ratio that is close to pyrolite (*86*). Segregation of this pyrolitic melt from the residual solid, followed by freezing of the melt at shallower depths, could lead to large-scale segregation of a mantle into a low-Mg/Si region above 23 GPa and a high-Mg/Si region at shallower depths. The latter rock will bear a higher abundance of periclase if it is returned to depth (>23 GPa) and would be substantially weaker than the rock that produced it, possibly penetrating to form weak channels or conduits to accommodate flow through the surrounding Mg-perovskite–rich rocks. This leads to a scenario very much like BEAMS, described earlier. However, such an escape clause via partial melting and segregation is only available if Mg/Si > 1 initially, because a planetary mantle with Mg/Si < 1 is expected to host Mg-perovskite along with a SiO_2 phase that is also expected to be highly viscous (*87*). In the latter case, eutectic melting and segregation do not lead to the production of any composition rock that is remarkably softer; thus, elevated temperatures would need to be maintained indefinitely to soften the rock sufficiently to release the internal heat of the planet. Such internal dynamics may determine whether a planet can sustain something like plate tectonics, which accommodates the interaction of internal matter with the surface environment, and sustain disequilibrium that is thought to be an important source of energy for sustaining a biosphere.

REFERENCES AND NOTES

1. N. Tomioka, K. Fujino, *Science* **277**, 1084–1086 (1997).
2. O. Tschauner *et al*., *Science* **346**, 1100–1102 (2014).
3. L. Liu, *Geophys. Res. Lett.* **1**, 277–280 (1974).
4. E. Ito, *Geophys. Res. Lett.* **4**, 72–74 (1977).
5. D. Yamazaki, S. Karato, *Am. Mineral.* **86**, 385–391 (2001).
6. W. Xu, C. Lithgow-Bertelloni, L. Stixrude, J. Ritsema, *Earth Planet. Sci. Lett.* **275**, 70–79 (2008).
7. A. Navrotsky, *Geophys. Res. Lett.* **7**, 709–711 (1980).
8. Y. Fukao, M. Obayashi, T. Nakakuki, *Annu. Rev. Earth Planet. Sci.* **37**, 19–46 (2009).
9. D. M. Trots *et al*., *J. Geophys. Res.* **118**, 5805–5813 (2013).
10. M. Murakami, K. Hirose, K. Kawamura, N. Sata, Y. Ohishi, *Science* **304**, 855–858 (2004).
11. A. R. Oganov, S. Ono, *Nature* **430**, 445–448 (2004).
12. T. Tsuchiya, J. Tsuchiya, K. Umemoto, R. A. Wentzcovitch, *Earth Planet. Sci. Lett.* **224**, 241–248 (2004).
13. R. M. Wentzcovitch, T. Tsuchiya, J. Tsuchiya, *Proc. Natl. Acad. Sci. U.S.A.* **103**, 543–546 (2006).
14. K. Ohta, K. Hirose, T. Lay, N. Sata, Y. Ohishi, *Earth Planet. Sci. Lett.* **267**, 107–117 (2008).
15. G. Fiquet *et al*., *Science* **329**, 1516–1518 (2010).
16. D. Andrault *et al*., *Earth Planet. Sci. Lett.* **293**, 90–96 (2010).
17. B. Grocholski, K. Catalli, S. H. Shim, V. Prakapenka, *Proc. Natl. Acad. Sci. U.S.A.* **109**, 2275–2279 (2012).
18. M. L. Rudolph, V. Lekić, C. Lithgow-Bertelloni, *Science* **350**, 1349–1352 (2015).
19. H. Marquardt, L. Miyagi, *Nat. Geosci.* **8**, 311–314 (2015).
20. S.-H. Shim *et al*., *Proc. Natl. Acad. Sci. U.S.A.* **114**, 6468–6473 (2017).
21. M. D. Ballmer, C. Houser, J. W. Hernlund, R. M. Wentzcovitch, K. Hirose, *Nat. Geosci.* **10**, 236–240 (2017).
22. K. Hirose, *J. Geophys. Res.* **107**, ECV 3-1–ECV 3-13 (2002).
23. S. Tateno, K. Hirose, N. Sata, Y. Ohishi, *Earth Planet. Sci. Lett.* **277**, 130–136 (2009).
24. T. Nakagawa, P. J. Tackley, *Geophys. Res. Lett.* **31**, L16611 (2004).
25. B. H. Hager, *J. Geophys. Res.* **89**, 6003–6015 (1984).
26. D. Yamazaki *et al*., *Phys. Earth Planet. Inter.* **228**, 262–267 (2014).
27. J. Girard, G. Amulele, R. Farla, A. Mohiuddin, S. Karato, *Science* **351**, 144–147 (2016).
28. D. P. Dobson *et al*., *Nat. Geosci.* **6**, 575–578 (2013).
29. C. A. McCammon, T. Stachel, J. W. Harris, *Earth Planet. Sci. Lett.* **222**, 423–434 (2004).
30. E. M. Smith *et al*., *Science* **354**, 1403–1405 (2016).
31. J. Badro *et al*., *Science* **300**, 789–791 (2003).
32. Z. Wu, R. M. Wentzcovitch, *Proc. Natl. Acad. Sci. U.S.A.* **111**, 10468–10472 (2014).
33. C. McCammon *et al*., *Nat. Geosci.* **1**, 684–687 (2008).
34. J. F. Lin *et al*., *Nat. Geosci.* **1**, 688–691 (2008).
35. A. Bengtson, J. Li, D. Morgan, *Geophys. Res. Lett.* **36**, L15301 (2009).
36. R. Sinmyo, C. McCammon, L. Dubrovinsky, *Am. Mineral.* **102**, 1263–1269 (2017).
37. H. Piet *et al*., *Proc. Natl. Acad. Sci. U.S.A.* **113**, 11127–11130 (2016).
38. J. M. R. Muir, J. P. Brodholt, *Phys. Earth Planet. Inter.* **257**, 12–17 (2016).
39. F. V. Kaminsky, J. F. Lin, *Am. Mineral.* **102**, 824–832 (2017).
40. Y. Tange, Y. Kuwayama, T. Irifune, K. Funakoshi, Y. Ohishi, *J. Geophys. Res.* **117**, B06201 (2012).
41. Y. Fei, L. Zhang, A. Corgne, H. Watson, A. Ricolleau, Y. Meng, V. Prakapenka, *Geophys. Res. Lett.* **34**, L17307 (2007).
42. S. Karato, K. Fujino, E. Ito, *Geophys. Res. Lett.* **17**, 13–16 (1990).
43. T. B. Ballaran *et al*., *Earth Planet. Sci. Lett.* **333-334**, 181–190 (2012).
44. Z. Mao *et al*., *Am. Mineral.* **102**, 357–368 (2017).
45. T. Katsura, A. Yoneda, D. Yamazaki, T. Yoshino, E. Ito, *Phys. Earth Planet. Inter.* **183**, 212–218 (2010).
46. J. Tsuchiya, T. Tsuchiya, R. M. Wentzcovitch, *J. Geophys. Res.* **110**, B02204 (2005).
47. G. M. Manthilake, N. de Koker, D. J. Frost, C. A. McCammon, *Proc. Natl. Acad. Sci. U.S.A.* **108**, 17901–17904 (2011).
48. K. Ohta *et al*., *Earth Planet. Sci. Lett.* **349-350**, 109–115 (2012).
49. H. Keppler, L. S. Dubrovinsky, O. Narygina, I. Kantor, *Science* **322**, 1529–1532 (2008).
50. A. F. Goncharov *et al*., *Phys. Earth Planet. Inter.* **247**, 11–16 (2015).
51. J. W. Hernlund, C. Thomas, P. J. Tackley, *Nature* **434**, 882–886 (2005).
52. Y. Ye, V. Prakapenka, Y. Meng, S. H. Shim, *J. Geophys. Res.* **122**, 3450–3464 (2017).
53. M. Murakami, Y. Ohishi, N. Hirao, K. Hirose, *Nature* **485**, 90–94 (2012).
54. A. Kurnosov, H. Marquardt, D. J. Frost, T. B. Ballaran, L. Ziberna, *Nature* **543**, 543–546 (2017).
55. R. M. Wentzcovitch, B. B. Karki, S. Karato, C. R. S. Da Silva, *Earth Planet. Sci. Lett.* **164**, 371–378 (1998).
56. X. L. Wang, T. Tsuchiya, A. Hase, *Nat. Geosci.* **8**, 556–559 (2015).
57. S. Cottaar, T. Heister, I. Rose, C. Unterborn, *Geochem. Geophys. Geosyst.* **15**, 1164–1179 (2014).
58. A. Kuvshinov, *Surv. Geophys.* **33**, 169–209 (2012).
59. T. Yoshino, S. Kamada, C. C. Zhao, E. Ohtani, N. Hirao, *Earth Planet. Sci. Lett.* **434**, 208–219 (2016).
60. K. Ohta *et al*., *Earth Planet. Sci. Lett.* **289**, 497–502 (2010).
61. R. Sinmyo, G. Pesce, E. Greenberg, C. McCammon, L. Dubrovinsky, *Earth Planet. Sci. Lett.* **393**, 165–172 (2014).
62. K. Ohta *et al*., *Science* **320**, 89–91 (2008).
63. R. Holme, *Geophys. J. Int.* **132**, 167–180 (1998).
64. S. Kakizawa, T. Inoue, H. Yurimoto, Goldschmidt 2015 Conference Abstracts, no. 1494 (Geochemical Society and the European Association of Geochemistry, 2015).
65. E. R. Hernández, D. Alfe, J. Brodholt, *Earth Planet. Sci. Lett.* **364**, 37–43 (2013).
66. J. E. Dixon, D. A. Clague, *J. Petrol.* **42**, 627–654 (2001).
67. N. Bolfan-Casanova, H. Keppler, D. C. Rubie, *Earth Planet. Sci. Lett.* **182**, 209–221 (2000).
68. J. P. Townsend, J. Tsuchiya, C. R. Bina, S. D. Jacobsen, *Earth Planet. Sci. Lett.* **454**, 20–27 (2016).
69. K. Yuan, B. Romanowicz, *Science* **357**, 393–397 (2017).
70. S. S. Shcheka, H. Keppler, *Nature* **490**, 531–534 (2012).
71. T. Komabayashi, K. Hirose, N. Sata, Y. Ohishi, L. S. Dubrovinsky, *Earth Planet. Sci. Lett.* **260**, 564–569 (2007).
72. L. Stixrude, C. Lithgow-Bertelloni, B. Kiefer, P. Fumagalli, *Phys. Rev. B* **75**, 024108 (2007).
73. T. Tsuchiya, J. Tsuchiya, *Proc. Natl. Acad. Sci. U.S.A.* **108**, 1252–1255 (2011).
74. K. Hirose, N. Shimizu, W. van Westrenen, Y. Fei, *Phys. Earth Planet. Inter.* **146**, 249–260 (2004).
75. A. Corgne, C. Liebske, B. J. Wood, D. C. Rubie, D. J. Frost, *Geochim. Cosmochim. Acta* **69**, 485–496 (2005).
76. D. Andrault *et al*., *Science* **344**, 892–895 (2014).
77. S. N. Perry, J. S. Pigott, W. R. Panero, *Am. Mineral.* **102**, 321–326 (2017).
78. N. Tsujino *et al*., *Nature* **539**, 81–84 (2016).
79. R. Nomura *et al*., *Rev. Sci. Instrum.* **88**, 044501 (2017).
80. S. Mukhopadhyay, *Nature* **486**, 101–104 (2012).
81. L. J. Hallis *et al*., *Science* **350**, 795–797 (2015).
82. A. Mundl *et al*., *Science* **356**, 66–69 (2017).
83. C. M. Bertka, Y. Fei, *Science* **281**, 1838–1840 (1998).
84. F. Sohl, G. Schubert, in *Treatise on Geophysics*, G. Schubert, Ed. (Elsevier, ed. 2, 2015), pp. 23–64.
85. D. C. Tozer, in *The Earth's Mantle*, T. F. Gaskell, Ed. (Academic Press, 1967), pp. 325–353.
86. C. Liebske, D. J. Frost, *Earth Planet. Sci. Lett.* **345-348**, 159–170 (2012).
87. F. Xu *et al*., *Earth Planet. Sci. Lett.* **459**, 332–339 (2017).
88. T. Ishii, H. Kojitani, M. Akaogi, *Earth Planet. Sci. Lett.* **309**, 185–197 (2011).
89. C. J. Allègre, J. P. Poirier, E. Humler, A. W. Hofmann, *Earth Planet. Sci. Lett.* **134**, 515–526 (1995).
90. A. Shahar *et al*., *Geochim. Cosmochim. Acta* **75**, 7688–7697 (2011).
91. N. Dauphas, F. Poitrasson, C. Burkhardt, H. Kobayashi, K. Kurosawa, *Earth Planet. Sci. Lett.* **427**, 236–248 (2015).
92. S. Tateno, K. Hirose, Y. Ohishi, *J. Geophys. Res.* **119**, 4684–4694 (2014).

ACKNOWLEDGMENTS

We thank the reviewers for their comments, which helped improve the manuscript. This research was supported by Japan Society for the Promotion of Science research grants (16H06285 to K.H. and 16H06023 and JP16H01115 to R.S.).

SUPPLEMENTARY MATERIALS

www.sciencemag.org/content/358/6364/734/suppl/DC1
Fig. S1
References (*93*–*97*)

10.1126/science.aam8561

Perovskite in Earth's deep interior

Kei Hirose, Ryosuke Sinmyo and John Hernlund

Science **358** (6364), 734-738.
DOI: 10.1126/science.aam8561